

Article

Dynamics of Muddy Rain of 15 June 2018 in Nepal

Ashok Kumar Pokharel ^{1,2,*}, Tianli Xu ¹, Xiaobo Liu ¹ and Binod Dawadi ^{1,3} 

¹ Kathmandu Center for Research and Education, Chinese Academy of Sciences-Tribhuvan University, Kathmandu 44613, Nepal; xutianli@itpcas.ac.cn (T.X.); xbliu@itpcas.ac.cn (X.L.); dawadibinod@gmail.com (B.D.)

² Weather Extreme Ltd., Incline Village, NV 89451, USA

³ Central Department of Hydrology and Meteorology, Tribhuvan University, Kathmandu 44613, Nepal

* Correspondence: ashokpokharel@hotmail.com

Received: 13 April 2020; Accepted: 15 May 2020; Published: 21 May 2020



Abstract: It has been revealed from the Modern-Era Retrospective analysis for Research and Applications MERRA analyses, Moderate Resolution Imaging Spectroradiometer MODIS/Terra satellite imageries, Naval Aerosol Analysis and Prediction System NAAPS model outputs, Cloud–Aerosol Lidar and Infrared Pathfinder Satellite Observations CALIPSO imageries, Hybrid Single Particle Lagrangian Integrated Trajectory HYSPLIT model trajectories, atmospheric soundings, and observational records of dust emission that there were multiple dust storms in the far western parts of India from 12 to 15 June 2018 due to thunderstorms. This led to the lifting of the dust from the surface. The entry of dust into the upper air was caused by the generation of a significant amount of turbulent kinetic energy as a function of strong wind shear generated by the negative buoyancy of the cooled air aloft and the convective buoyancy in the lower planetary boundary layer. Elevated dust reached a significant vertical height and was advected towards the northern/northwestern/northeastern parts of India. In the meantime, this dust was carried by northwesterly winds associated with the jets in the upper level, which advected dust towards the skies over Nepal where rainfall was occurring at that time. Consequently, this led to the muddy rain in Nepal.

Keywords: thunderstorm; dust storm; muddy rain; transport; convection; buoyancy; turbulent kinetic energy

1. Introduction

It has been found that the lofted dust from wind erosion causes environmental effects at regional and global scales. Atmospheric dust affects climate globally by altering the radiation balance of the atmosphere [1,2]. Similarly, high concentrations of dust cause negative health effects [3,4] as well as, on a regional scale, lower economic status by deteriorating visibility with an increase in the cost of visibility impairment on national parks and wilderness areas. A positive correlation has been indicated between drought years and increased dust lofting [5], whereas others indicated that the intrusion of dust into the atmosphere occurs when freshly deposited sediment caused by the intense storms becomes dried up [6]. A dust climatology study over the southwestern US mentioned that the annual mean number of dust events, the annual mean duration of dust events, and the ratio of duration to number of dust events was directly proportional to the visibility range [7]. This study also found that the higher the percentage of total seasonal precipitation, the lower the total dust events percentage in the summer and the winter, and the lower the percentage of total seasonal precipitation, the higher the total dust event percentage in the spring and the autumn.

It has been stated that the capability of the wind to deflate the dust particles (erosivity), the soil's susceptibility to entrainment (erodibility), and the supply of erodible sediment are three major controlling factors on the dust emission process [8]. It is found that the downslope winds and the

unbalanced adjustment processes in the lee of the mountain ranges are the terrain-induced wind storms that also lift the dust from the surface, and produce larger-scale dust aerosol mobilization, and transport [9–13].

On the other hand, there are some examples that show thunderstorms produce very strong downburst winds leading to dust storms (i.e., strong and turbulent wind events by which dust is lofted from the surface and carries clouds of fine dust, soil, and sand over a large area) [14]. In happening thus, the wall of dust created by this kind of storm can be miles long and several thousand feet high [15]. In southwest Asia, dust storm activity is also controlled by thunderstorm occurrence, lifting dust from the ground surface. Though the highest frequency of thunderstorms is during the wet months—July and August,—there is also substantial thunderstorm activity in May and June, prior to major precipitation occurrence over this region [16]. Similarly, dust storms are most frequent in the afternoon, when turbulent mixing is most pronounced, due to the abundant insolation. This was found in Mexico Basin, where events were associated with strong downdraughts generated by the convective process-dry thunderstorms [17]. As far as the thunderstorm over Nepal is concerned, lightning activity starts in March; it intensifies quickly, reaching its peak in May, while in June the activity decreases rapidly as the southwest monsoon starts [18].

Due to extreme dust storms of 28 March 2016 over Kathmandu, Nepal and its surrounding areas there was a significant reduction in visibility (2 km), effects in aviation and ground transportation, and air quality deterioration. This reveals how vulnerable Nepal is to dust storm and how severely dust storms affect Nepal. On the other hand, unfortunately there are a lack of studies about the origin of dust storms, transport and deposition of dust, and a detailed understanding of the climatological and meteorological characteristics that influence dust event frequency and dust rain dynamics in Nepal. This type of knowledge is necessary to understand the regional, local dust climatology, and the atmospheric phenomena that affect the transport and deposition of the dust in Nepal. In this regard, the study of recent muddy rain (a kind of rain which contains enough dust (e.g., desert dust) to be clearly visible. This occurs when dust and dirt particles mix with the rain [19] of 15 June 2018 in Nepal, which might have increased the pH of rain water, has become quite a newsworthy issue as it is a quite unusual activity over Nepal and its neighbors, and the dust particles can neutralize acid rain in a manner similar to the way antacids counteract excess acid in an upset stomach [20]. For example, the increased level of pH was observed in southern Corsica in 1984 when the chemistry of precipitation mixed with Saharan dust was analyzed [21]. It is to be noted here that based on the findings of previous studies increase of pH has been suspected during this particular muddy rain. However, this study does not incorporate any discussion of the possible impacts of pH caused by this particular event due to beyond the scope of the study.

According to Meteorological Forecasting Division (MFD) of Nepal, there was a muddy rain over Nepal on 15 June 2018 [22], which was also observed by the public, as shown in Figure 1. They did not discuss the detailed atmospheric dynamics regarding the processes responsible for causing that muddy rain. To address these issues, this study is accomplished, which describes different processes below. As far as the previous studies of detail atmospheric dynamics of muddy rain in Nepal are concerned, no such studies have been carried out in Nepal. For the first time, this study will reveal the scientific understanding of muddy rain dynamics over Nepal.

Nepal is situated between China in the north and India to the south, east and west (i.e., 26.37°–30.07° N and 80.07°–88.20° E). It is a country of tremendous geographic diversity. Elevation ranges from 59 m in Terai to Earth's highest point, the 8848 m Mount Everest. It has a warm temperate climate with dry winters and hot summers. Average annual precipitation ranges from 160 to 5500 mm.



Figure 1. Red arrow indicates deposited dust on leaves [23].

2. Methodology

For this study, surface meteorological data and a map of regional overview of Indian subcontinent were collected from the Department of Meteorology and Hydrology, Nepal (DHM-Nepal) and weatherunderground.com [24,25]. Satellite imagery from Moderate Resolution Imaging Spectroradiometer (MODIS)/Terra [26] were collected and analyzed in depth. For the synoptic scale observational atmospheric processes analysis, the reanalysis datasets of surface pressure, geopotential height, air temperature, precipitable water, wind speed and direction, and vertical motion obtained from the Modern Era Retrospective-Analysis for Research and Applications (MERRA) ($0.50^\circ \times 0.67^\circ$) were used to make horizontal cross sections [27]. Vertical cross sections of wind speed components and potential temperature were plotted from the selected reanalysis datasets. An evolution of the dust by an aerosol modelling system at $1^\circ \times 1^\circ$ horizontal resolution from the Navy Aerosol Analysis and Prediction System (NAAPS) [28] was considered. In addition to this, Modern-Era Retrospective Analysis for Research and Applications-2 (MERRA-2) model (spatial resolution $0.5^\circ \times 0.625^\circ$) hourly datasets were used to analyze the dust scattering aerosol optical thickness (AOT) 550 nm of $1 \mu\text{m}$ particulate matter [29] over this region of interest. Rawinsonde data were obtained from the University of Wyoming, USA [30]. Similarly, the dust backward trajectories were analyzed using the Hybrid Single Particle Lagrangian Integrated Trajectory (HYSPPLIT) model [31]. To analyze the vertical reach of dust, imageries of Cloud-Aerosol Lidar and Infrared Pathfinder Satellite Observation (CALIPSO) [32] were also taken into account.

3. Results and Discussion

3.1. Observation of Dust Storms from Some Surface Stations

Locations of surface stations close to the area of dust storms is shown in the regional overview of Indian subcontinent (Figure 2) [24,25]. Observational data of Safdarjung Airport, India ($28.58^\circ \text{ N } 77.21^\circ \text{ E}$) and Sardar Vallabhbhai Patel International Airport, India ($23.07^\circ \text{ N } 72.63^\circ \text{ E}$) archived by Weather Underground (Table 1) indicated that dust storms hit Safdarjung Airport, India at 5:45 to 8:45 a.m. (local time) on 12 June 2018 with westerly/west-northwesterly winds ranging from 6.26 to 8.05 m s^{-1} speed; at 5:45 to 11:45 a.m. on 13 June 2018 with westerly wind ranging from 7.60 to 9.39 m s^{-1} ; at 3:45 to 8:45 a.m. on 14 June 2018 with west-southwesterly wind ranging from 4.47 to 7.15 m s^{-1} ; and at 3:45 to 5:45 a.m. on 15 June 2018 with west/west-southwesterly winds ranging from 6.26 to 7.60 m s^{-1} speed. Similarly, Sardar Vallabhbhai Patel Intl Airport, India experienced dust storms at 6:45 to 11:45 a.m. (local time) of 12 June 2018 with westerly/southwesterly/west-southwesterly

winds ranging from 4.02 to 5.36 m s⁻¹; at 4:15 a.m. to 11:15 p.m. (local time) of 13 June 2018 with westerly/southwesterly/west-southwesterly winds ranging from 2.68 to 6.26 m s⁻¹; at 12:45 a.m. to 11:15 p.m. (local time) of 14 June 2018 with south-southwesterly/west-southwesterly winds ranging from 2.68 to 7.15 m s⁻¹; and at 5:45 a.m. to 5:45 p.m. (local time) of 15 June 2018 with southwesterly/south-southwesterly/west-southwesterly winds ranging from 2.68 to 7.70 m s⁻¹. Hence, this clearly shows that there were multiple dust storms in the far western parts of India from 12 to 15 June of 2018. It is to be noted here that prior to these event days (e.g., 10–11 June 2018), there was no precipitation and the flow of strong wind at Safdarjung Airport and Sardar Vallabhbhai Patel International Airport, India.

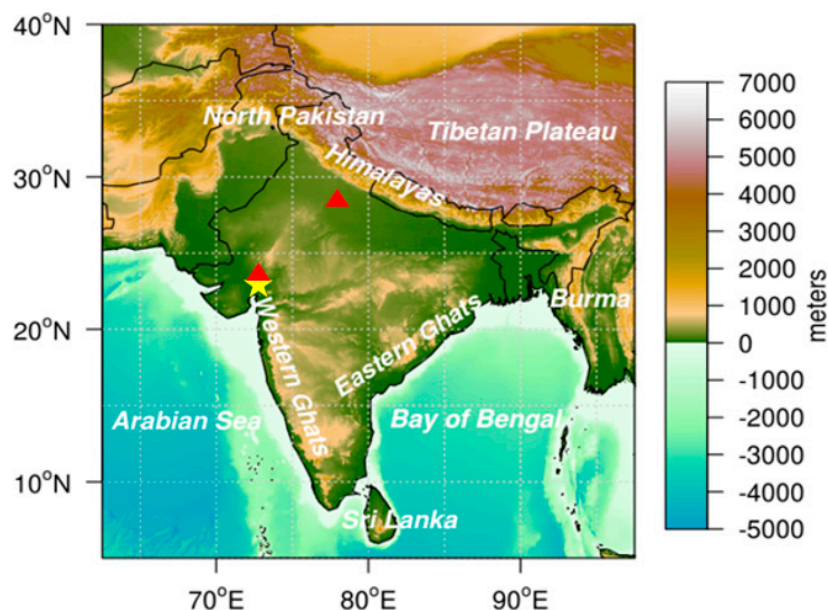


Figure 2. Observation of dust storms from some surface stations are shown by red coloured triangles in the map of regional overview of Indian subcontinent [24,25]. A triangle, which is shown in the side of Himalyas, represents Safdarjung Airport, India, and another triangle represents Sardar Vallabhbhai Patel International Airport, India. Rawinsonde sounding station at Ahamadabad in India is also shown by a yellow coloured star.

Table 1. Surface weather data observed at two stations of India [24].

Name of Surface Stations	Date of Dust Storms	Local Time	Wind Speed (m s ⁻¹)	Wind Direction
Safdarjung Airport, India	12 June 2018	5:45 a.m. to 8:45 a.m.	6.26 to 8.05	Westerly/West-northwesterly
	13 June 2018	5:45 a.m. to 11:45 a.m.	7.60 to 9.39	Westerly
	14 June 2018	3:45 a.m. to 8:45 a.m.	4.47 to 7.15	West-southwesterly
	15 June 2018	3:45 a.m. to 5:45 a.m.	6.26 to 7.60	West/west-southwesterly
Sardar Vallabhbhai Patel International Airport, India	12 June 2018	6:45 a.m. to 11:45 a.m.	4.02 to 5.36	Westerly/Southwesterly/West-southwesterly
	13 June 2018	4:15 a.m. to 11:15 p.m.	2.68 to 6.26	Westerly/Southwesterly/West-southwesterly
	14 June 2018	12:45 a.m. to 11:15 p.m.	2.68 to 7.15	South-southwesterly/West-southwesterly
	15 June 2018	5:45 a.m. to 5:45 p.m.	2.68 to 7.70	Southwesterly/South-southwesterly/West-southwesterly

3.2. Dust Storms and the Dust Advection

The MODIS/Terra images [26] captured useful images of massive dust storms of thick dust over the far West to Northwest to North of India from 12 June to 15 June 2018, as shown in Figure 3a–d, respectively. Although these figures are not able to indicate the exact location and the time of the initiation of the dust storm, based on the earliest available images among them and observational

information, it can be inferred that the first lifting of dust was initiated around 26.3° N 73.01° E on 12 June 2018 (Figure 3a).

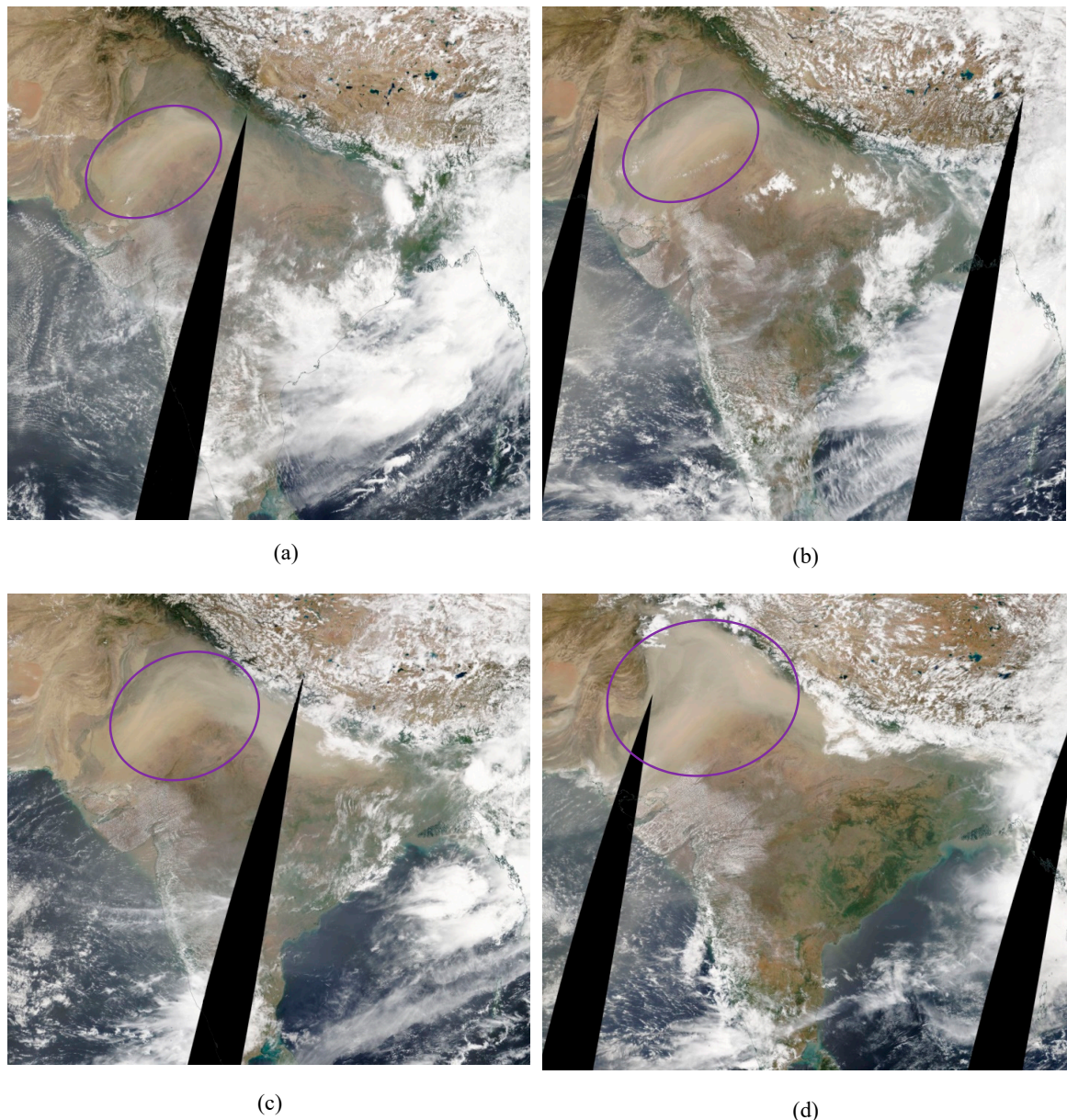


Figure 3. Dust storms images captured by moderate resolution imaging spectroradiometer (MODIS)/Terra (1 km resolution) on 12–15 June 2018 ((a–d), respectively [26]). Pink colored circles area show the dust plume areas of western to northwestern to northern parts of India.

3.3. Synoptic Overview from the MERRA

Based on the $0.50^{\circ} \times 0.67^{\circ}$ MERRA reanalysis datasets [27], a meso- α /synoptic observational analysis was carried out to find out the roles of different atmospheric processes from the surface to the mid-troposphere at different time intervals that may have generated this particular favorable muddy rain environment. The mid tropospheric synoptic overview from the MERRA shows that there was a positively tilted trough (oriented along a southwest-northeast axis) in the far western/southwestern parts of India and southwestern/southern parts of Nepal from 12 June 2018 (Figure 4a). Over time, the geopotential height consistently showed a positively tilted trough (the presence of trough indicates the condition of static instability below it, the generation of strong positive vorticity advection, and the

creation of differential temperature advection (i.e., upper level and low-level fronts)) with falling heights rotated cyclonically to be oriented more southern to southwestern across Nepal till 15 June 2018 (Figure 4b). On 0630 UTC of 12 June 2018 a jet at 500 hPa (causes the upper level forcing) was propagating from northwest of India to western to southern to eastern parts of Nepal, respectively, with further amplification over time; therefore, it was continuously advancing on its way, influencing the trough. The baroclinic amplification of the jet streak was consistent with the deepening of the trough at that time. Similarly, on 0000 UTC of 15 June 2018, there were a juxtaposition of the jet with lower level mesoscale jetlet between 700 and 850 hPa, referring to a possible coupling between the upper and lower level wind maxima. Due to the presence of the upper level trough and the strong jet over our region of interest it can be inferred that the combination of these lift mechanisms played significant roles for occurrence of thunderstorms leading to downburst, kicking up the dust (Figure 3a–d), and carrying the lofted dust into Nepal for causing a muddy rainfall over there. These processes are also discussed in different sub-sections below.

3.4. Evolution of the Dust by an Aerosol Modeling of Navy Aerosol Analysis and Prediction System (NAAPS) and Dust Scattering AOT by MERRA-2

The NAAPS model is an additional supporting information regarding the occurrence of dust storm data in aforesaid region of few observations. It is a $1^\circ \times 1^\circ$ resolution aerosol model that depicts dust predictions at 6-h intervals [28], is also used to diagnose the beginning and subsequent multiple occurrences of dust storms over our region of interest. This model reveals the evolution of the dust, including the concentration of sulfate over the region, and it can be related to the strength and track of the dust transport over time. It is important to note that sulfate was associated with the initial emission of the dust into the atmosphere, and over time, due to the lower density associated with sulfate compared with dust it remains for a relatively long period of time in the environment. Though the concentration of sulfate is lower than the dust in the composite form of the initial emission of the total material from the surface, over time, sulfate can be recognized due to its longevity in the atmosphere more than the dust due to its lower density. Here, we analyzed the NAAPS aerosol modeling image from 0000 UTC of June 12 to 15, 2018. NAAPS shows that the strongest signal of dust and sulfate emission into the atmosphere was largely over the $20\text{--}22^\circ \text{ N } 68\text{--}74^\circ \text{ E}$ region at 0600 to 1800 UTC of 13 June 2018 (Figure 5a–b). At 1800 UTC of 14 June 2018 and onwards, the strength and areal extension of the dust and sulfate materials increased and mostly advected towards the northwest/north/northeast region of India and its neighbors, $22\text{--}35^\circ \text{ N } 68\text{--}88^\circ \text{ E}$ (Figure 5c). Similarly, MERRA-2 model shows that the dust-scattering AOT reached up to 0.874 when the intrusion of dust reached in maximum vertical height in early of 14 June 2018 in the western parts of Nepal; and over time this value was diluted [29] when the dust was advected towards the eastern parts of Nepal.

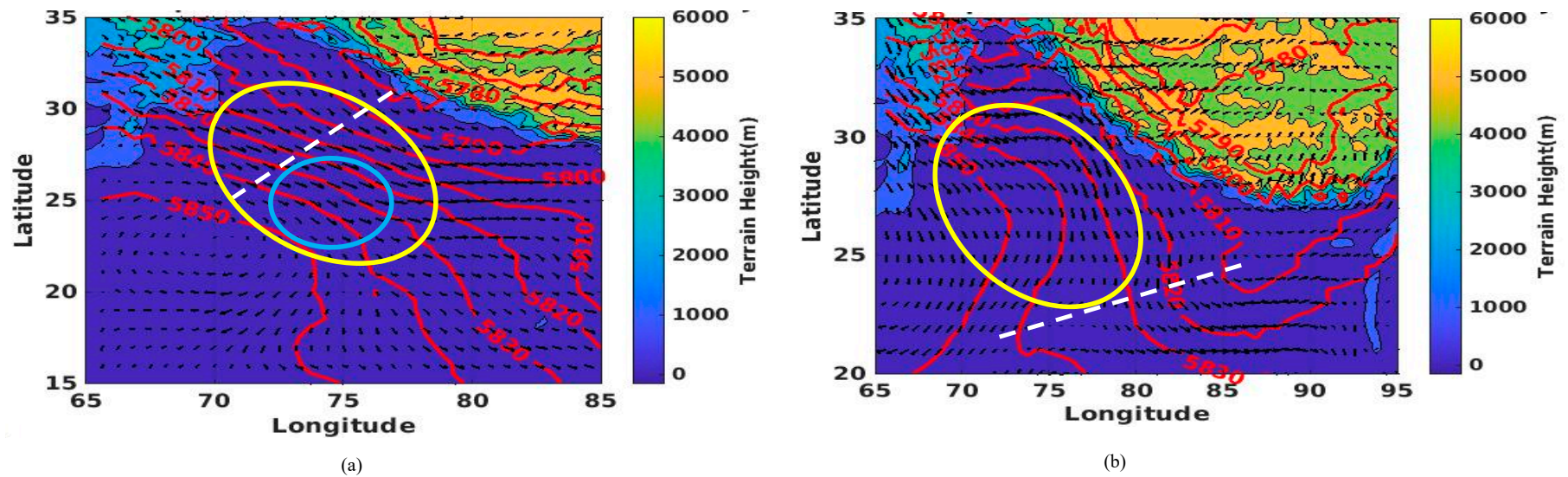


Figure 4. (a) Geopotential height and wind speed/direction at 500 hPa at 0630 UTC on 12 June 2018. The yellow colored circle shows the flow of jet and the white dotted line indicates a trough axis from the Modern-Era Retrospective analysis for Research and Applications MERRA reanalysis with horizontal resolution of $0.5^\circ \times 0.67^\circ$ [27]. The light blue colored circle shows the area of dust storm and the thunderstorm outbreak; (b) Geopotential height and wind speed/direction at 500 hPa on 0930 UTC on 15 June 2018. The yellow colored circle shows the flow of jet and the white dotted line indicates a trough axis from the Modern-Era Retrospective analysis for Research and Applications (MERRA) reanalysis with horizontal resolution of $0.5^\circ \times 0.67^\circ$ [27].

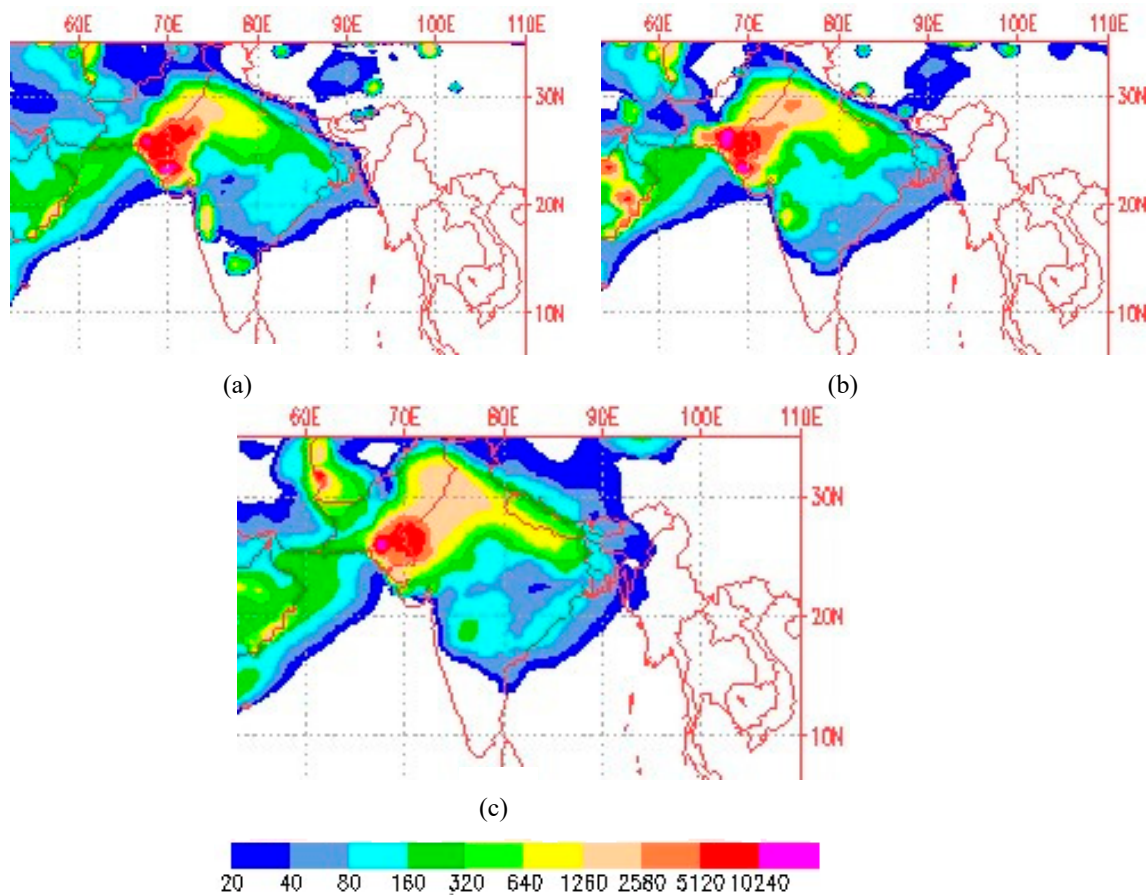


Figure 5. (a) Dust concentration ($\mu\text{g}/\text{m}^3$) at 0060 UTC on 13 June 2018 (Green and yellow show the dust and red shows sulfate (horizontal resolution of $1^\circ \times 1^\circ$)) [28]; (b) Dust concentration ($\mu\text{g}/\text{m}^3$) at 1200 UTC on 13 June 2018 (Green and yellow show the dust and red shows sulfate (horizontal resolution $1^\circ \times 1^\circ$)) [28]; (c) Dust concentration ($\mu\text{g}/\text{m}^3$) at 1800 UTC on 14 June 2018 (Green and yellow show the dust and red shows sulfate (horizontal resolution of $1^\circ \times 1^\circ$)) [28].

3.5. Rawinsonde Soundings Analyses

To observe the vertical temperature and wind speed/direction profiles at different atmospheric pressure levels close to the time period of the muddy rainfall in Nepal, the rawinsonde sounding of Ahamadabad (23.06° N , 72.63° E) in India obtained from University of Wyoming, USA [30] was analyzed from 12–15 June 2018 (Figure 6). Since this sounding station is close to the possible dust sources we expect that the information regarding the vertical profiles of different meteorological variables from these stations could be well represented in this analysis. A sounding at Ahamadabad (23.06° N 72.63° E), which is close to the possible area of a dust storm, at 1200 UTC of June 12, 2018 shows the likely condition of a thunderstorm because of the value of the convective available potential energy (CAPE) ($1438 \text{ J}/\text{kg}$) and the lifted index (-9.76) at that time (i.e., responsible for lifting mechanism), generation of the trigger effect due to the presence of warm air and moisture at a lower level (shown by the value of the dew point, which is greater than 21° C and veering directional change of wind 45° or more from surface to 700 hPa, 850 to 700 hPa wind was $10.3 \text{ m}/\text{s}$ (i.e., low-level jet) or greater in the observed sounding), and the presence of the trough and jet as discussed in the earlier section. Hence, there was a combination of high planetary boundary layer (PBL) moisture, strong directional and wind shear, low convective inhibition, CAPE, and lifting mechanisms.

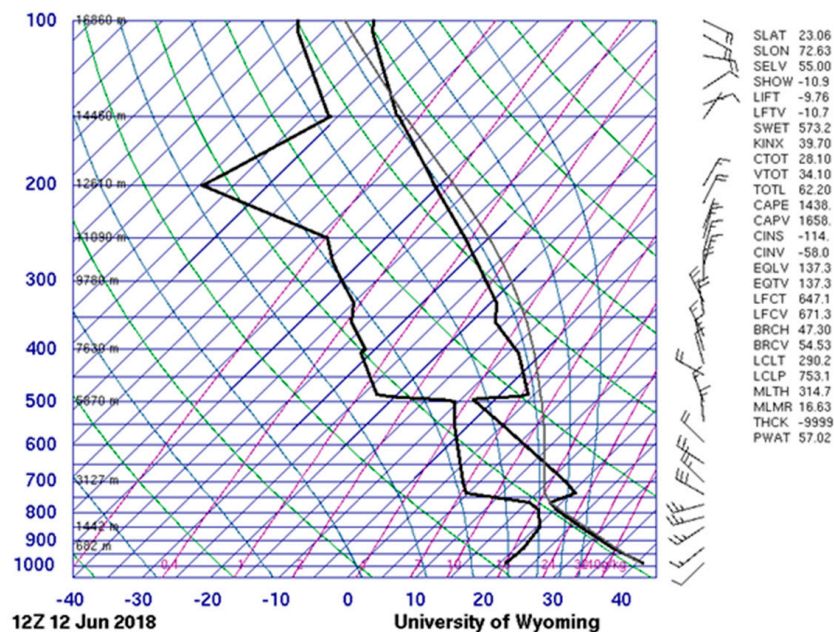


Figure 6. Atmospheric sounding observed at Ahamadabad, India at 1200 UTC on 12 June 2018 [30].

In addition to this, the sounding, which is presented in Figure 6, is inverted and “V”-shaped and is also showing that the dew point depression decreased significantly with height, dry air (low RH) in the lower troposphere with nearly saturated air (high RH) in the middle troposphere, the presence of inversion separating the dry air aloft and the moist air near the surface, and the convective condensation level (CCL) at a high elevation. Hence, this “V”-shaped sounding reveals that there was a quite appropriate condition for the generation of a strong downdraft from the severe thunderstorm. For example, when an inversion (also known as cap) existed from the surface to a certain height, heat, moisture, and instability could have built under this “capping” inversion. Over time, once the cap broke due to the addition of daytime sensible heating, then explosive convection occurred resulting in wind gusts. This was due to the entrain of dry air aloft into the downdraft. This promoted evaporative cooling and further enhanced the negative buoyancy of a parcel. In this case, a cold parcel of air surrounded by warm air descended faster than the surrounding air since the cold air was denser, and cooler air is often noticed at the surface when the downburst air reaches the observer. When this cooler air interacted with the warm buoyant air column present in the lower troposphere, as indicated by the sounding above, there was a lifting of the dust to 740 hPa and upward caused by the generation of the significant amount of turbulent eddies. This turbulence was the result of the summation of the strong wind shear and the buoyancy, as suggested by [33]. All these aforesaid processes were consequences of the thunderstorm and its effect in Ahamadabad and its surroundings. This is consistent with the observation of dust storm observed at Sardar Vallabhbai Patel Intl Airport, India (23.07° N, 72.63° E), which is very close to this sounding station in Ahamadabad, as already mentioned in the earlier section.

3.6. Analyses of Backward Trajectory and Vertical Reach of Dust

The HYSPLIT model is run with full ensemble set-up, producing a variety of parcel back trajectories [31], as shown in Figure 7. It is used here to compute air parcel trajectories and the deposition or dispersion of lofted dust from the source of dust to recipient of it (e.g., to find out where did the dust come from to Nepal). In other words, this is used here to establish whether a high level of dust at one location (e.g., Nepal) is caused by the transport of air contaminants from another location. For this analysis, Kathmandu (27.72° N, 85.32° E) in Nepal is considered as a recipient point.

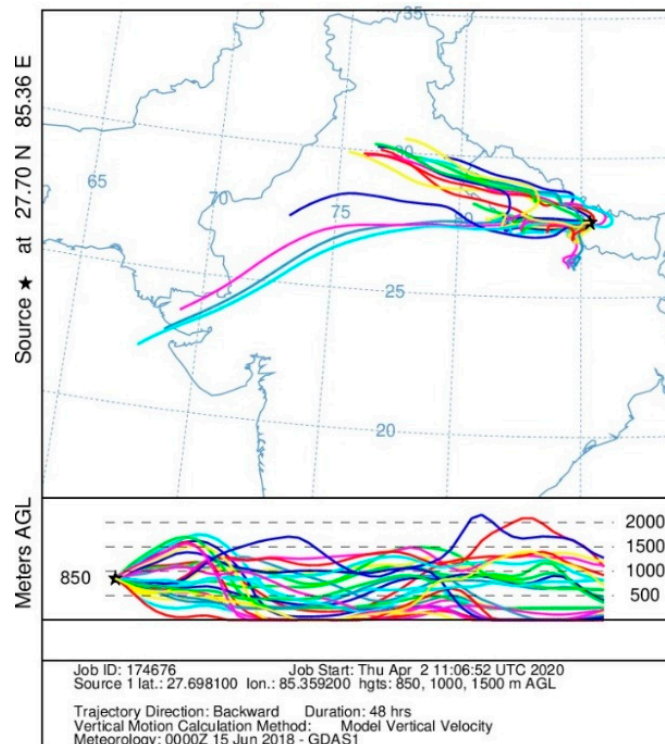
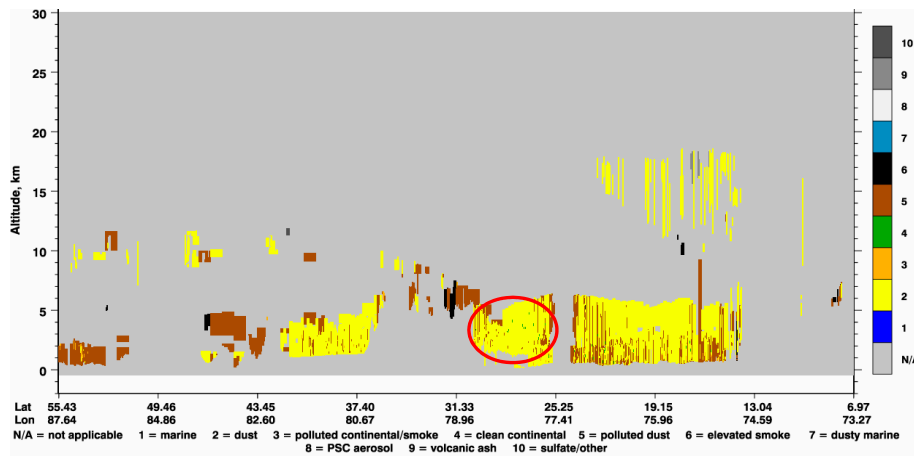


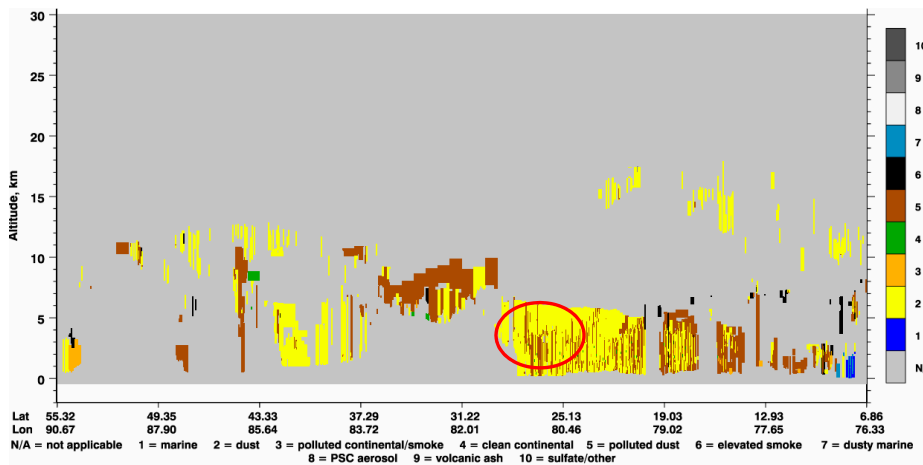
Figure 7. Backward Trajectory by the Hybrid Single Particle Lagrangian Integrated Trajectory (HYSPLIT) model [31] ending at 2300 UTC on 15 June 2018.

HYSPLIT back trajectories of 10 to 16 June of 2018 combined with MODIS satellite imageries have provided insight into whether high muddy rain was caused by local air pollution sources or whether dust was blown in the wind. Further, the backward trajectories (Figure 7) clearly infer that the air parcel laden with dust was transported from the western parts (between 22° N 72° E and 27° N to 77° E) of India to Nepal (e.g., Kathmandu), as shown by the higher air currents. This also reveals that Thar desert of both Rajasthan and Gujarat states of India, which lie in the western part of India, served as a dust source in this particular event.

This is also supported by CALIPSO images [32], which show that the vertical reach of dust was 6 km (Figure 8a,b). This infers that when the dust reached such a height, the strong westerly/northwesterly current of air at that height, as discussed in an earlier section, advected dust towards the sky of Nepal, where the precipitable water was present at that time (Figure 9), leading to muddy rain in Nepal.



(a)



(b)

Figure 8. (a) Vertical stretch of dust at 20:42:26.8 to 20:55:55.4 UTC on 13 June 2018 captured by CALIPSO [32]. The red circled area shows vertical reach of dust; (b) Vertical stretch of dust at 20:30:08.0 to 20:43:36.7 UTC on 15 June 2018 captured by CALIPSO. The red circled area shows vertical reach of dust.

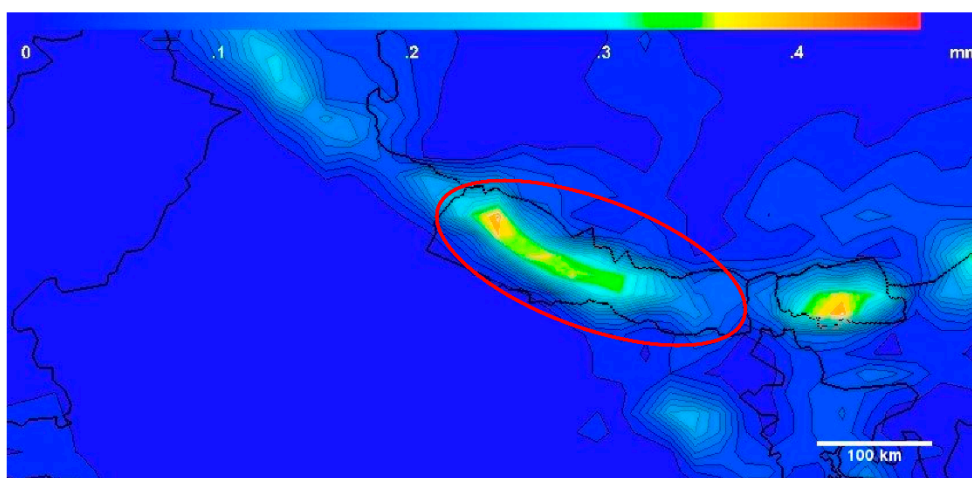


Figure 9. Total precipitable water in mm (shown in legend at upper part of Figure) over Nepal (shown by a red coloured circle area) at 1830 UTC on 15 June 2018 from the MERRA reanalysis with horizontal resolution of $0.5^\circ \times 0.67^\circ$.

4. Conclusions

There were big surges of dust storms in the far western parts of India, especially Ahamadabad and its surroundings, caused by thunderstorms from 12 to 15 June 2018, intermittently. There was a lifting of dust into the upper air caused by the generation of significant amount of turbulent kinetic energy as a function of strong gust wind, which had strong wind shear, and the convective buoyancy at the lower boundary layer during the descending outflow of cold air caused by the generation of a severe thunderstorm. When this lofted dust in the upper air came into contact with prevailing winds, such as northwesterly/westerly associated with the jets, as discussed in the earlier sections, upper air dust was advected towards Nepal, where rainfall was occurring, led to the muddy rain in Nepal. Hence, the study of this particular event reveals that western parts of India were dust source regions (i.e., Thar desert of both Rajasthan and Gujarat states of India, which plays a significant role as a source of emission of dust caused by the dust storms during the months of March–June every year [34]) from which dust was transported to Nepal as a long range transport. As this finding is still based on the low-resolution datasets, it would be better if it could be done on the high-resolution datasets so that the details of finer temporal and spatial processes, such as emission to transport to the deposition of dust in this particular event, could be further understood. In addition to this, there is a need for more cases in order to establish the representativeness of the event presented here.

Author Contributions: Conceptualization, methodology, software, validation, formal analysis, investigation, and writing, A.K.P.; resources and project administration, T.X., X.L., and B.D. All authors have read and agreed to the published version of the manuscript.

Funding: This research is funded by Kathmandu Center for Research and Education (KCRE), Chinese Academy of Sciences (CAS)—Tribhuvan University (TU).

Acknowledgments: We would like to thank Tandong Yao and Tao Wang for their helpful advice and support. Also, thanks goes to Kathmandu Center for Research and Education, Chinese Academy of Sciences-Tribhuvan University, Kathmandu, Nepal for providing financial support for this study.

Conflicts of Interest: The authors declare no conflict of interest.

References

1. Seinfeld, J.; Carmichael, G.; Arimoto, R.; Conant, W.; Brechtel, F.; Bates, T.; Cahill, T.; Clarke, A.; Doherty, S.; Flatau, P.; et al. ACE-ASIA: Regional climatic and atmospheric chemical effects of Asian dust and pollution. *Bull. Am. Meteor. Soc.* **2004**, *85*, 367–380. [[CrossRef](#)]
2. Tegen, I. Modeling the mineral dust aerosol cycle in the climate system. *Quat. Sci. Rev.* **2003**, *22*, 1821–1834. [[CrossRef](#)]
3. Appel, B.; Tokiwa, Y.; Hsu, J.; Kothny, E.; Hahn, E. Visibility as related to atmospheric aerosol constituents. *Atmos. Environ.* **1985**, *19*, 1525–1534. [[CrossRef](#)]
4. Chan, Y.; Simpson, R.; Mctainsh, G.; Vowles, P.; Cohen, D.; Bailey, G. Sourceapportionment of visibility degradation problems in Brisbane (Australia)—Using the multiple linear regression techniques. *Atmos. Environ.* **1999**, *33*, 3237–3250. [[CrossRef](#)]
5. Okin, G.S.; Reheis, M.C. An ENSO predictor of dust emission in the southwestern United States. *Geophys. Res. Lett.* **2002**, *29*. [[CrossRef](#)]
6. Reheis, M.; Kihl, R. Dust deposition in southern Nevada and California, 1984–1989: Relations to climate, source area, and source lithology. *J. Geophys. Res.* **1995**, *100*, 8893–8918. [[CrossRef](#)]
7. Pokharel, A.; Kaplan, M. Dust Climatology of the NASA Dryden Flight Research Center (DFRC) in Lancaster, California, USA. *Climate* **2017**, *5*, 15. [[CrossRef](#)]
8. Okin, G.S.; Gillette, D.A.; Herrick, J.E. Multi scale controls on and consequences of Aeolian process in landscape change in arid and semi-arid environments. *J. Arid Environ.* **2006**, *65*, 253–275. [[CrossRef](#)]
9. Pokharel, A.; Kaplan, M.; Fiedler, S. Subtropical Dust Storms and Downslope Wind Events. *J. Geophys. Res. Atmos.* **2017**, *122*, 10. [[CrossRef](#)]
10. Pokharel, A.; Kaplan, M. Organization of dust storms and synoptic scale transport of dust by Kelvin waves. *Earth Syst. Dynam.* **2019**, *10*, 651–666. [[CrossRef](#)]

11. Pokharel, A.; Kaplan, M.; Fiedler, S. The Role of Jet Adjustment Processes in Subtropical Dust Storms. *J. Geophys. Res. Atmos.* **2017**, *122*, 12. [CrossRef]
12. Pokharel, A.; Kaplan, M.; Fiedler, S. Atmospheric Dynamics of the Harmattan Surge on March 2, 2004. In Proceedings of the 2nd International Conference on Atmospheric Dust–DUST 2016, Taranto, Italy, 12–17 June 2016; pp. 85–93. [CrossRef]
13. Pokharel, A. Atmospheric Dynamics of Sub-Tropical Dust Storms. Ph.D. Thesis, University of Nevada, Reno, USA, 2016. Available online: <https://ui.adsabs.harvard.edu/abs/2016PhDT98P/abstract> (accessed on 3 February 2020).
14. Brazel, A.; HSU, S. The climatology of hazardous Arizona dust storms. *Desert Dust* **1981**, *186*, 293–303. [CrossRef]
15. SciJinks. Available online: <https://scijinks.gov/dust-storm/> (accessed on 3 February 2020).
16. Goudie, A.; Middleton, N. Dust storms in South West Asia. *Acta Universitatis Carilinae Suppl.* **2000**, 73–83.
17. Jauregui, E. The dust storms of Mexico City. *Int. J. Climatol.* **1989**, *9*, 169–180. [CrossRef]
18. Baral, K.N.; Mackerras, D. The cloud flash-to-ground flash ratio and other lightning occurrence characteristics in Kathmandu thunderstorms. *J. Geophys. Res.* **1992**, *97*, 931–938. [CrossRef]
19. Zifa, W.; Hiromasa, U. *Modelling of Long Range Transport of Yellow Sand and Muddy Rain in East Asia*; Annuals of Disasters Prevention Research Institute, Kyoto University: Kyoto, Japan, 1999; No. 42 B-1.
20. Hedin, L.; Likens, G. Atmospheric Dust and Acid Rain. *Sci. Am.* **1996**, *275*, 88–92. [CrossRef]
21. Loje-Pilot, M.D.; Martin, J.M.; Morelli, J. Influence of Saharan dust on the rain acidity and atmospheric input to the Mediterranean. *Nature* **1986**, *321*, 427–428. [CrossRef]
22. The Himalayan. Available online: <http://thehimalayantimes.com/nepal/kathmandu-valley-receives-muddy-rain/> (accessed on 3 February 2020).
23. Twitter. Available online: <https://twitter.com/rupajoshi/status/1007806022805700608/photo/1> (accessed on 3 February 2020).
24. Weather Underground. Available online: Weatherunderground.com (accessed on 3 February 2020).
25. Stolbova, V.; Martin, P.; Bookhagen, B.; Marwan, N.; Kurths, J. Topology and seasonal evolution of the network of extreme precipitation over the Indian subcontinent and Sri Lanka. *Nonlin. Processes Geophys.* **2014**, *21*, 901–917. [CrossRef]
26. MODIS/Terra. Available online: <https://worldview.earthdata.nasa.gov> (accessed on 3 February 2020).
27. MERRA. Available online: https://disc.sci.gsfc.nasa.gov/mdisc/data-holdings/merra/merra_products_nonjs.shtml (accessed on 3 February 2020).
28. NAAPS. Available online: https://www.nrlmry.navy.mil/aerosol_web/ (accessed on 3 February 2020).
29. MERRA-2/Giovanni. Available online: <https://giovanni.gsfc.nasa.gov/giovanni/> (accessed on 3 February 2020).
30. University of Wyoming sounding. Available online: <http://weather.uwyo.edu/upperair/sounding.html> (accessed on 3 February 2020).
31. HYSPLIT. Available online: <https://www.ready.noaa.gov/HYSPLIT.php> (accessed on 5 March 2020).
32. CALIPSO. Available online: https://www-calipso.larc.nasa.gov/tools/data_avail/index.php?d=2018 (accessed on 5 March 2020).
33. Stull, R. *Meteorology for Scientists and Engineers*, 2nd ed.; Brooks Cole: Pacific Grove, CA, USA, 1999.
34. Sarkar, S.; Chauhan, A.; Kumar, R.; Singh, R.P. Impact of deadly dust storms (May 2018) on air quality, meteorological, and atmospheric parameters over the northern parts of India. *GeoHealth* **2019**, *3*, 67–80. [CrossRef] [PubMed]

